1   **Mercury distribution in the upper troposphere and lowermost**

2   **stratosphere according to measurements by the IAGOS-CARIBIC**

3   **observatory, 2014-2016**

6   Franz Slemr[1], Andreas Weigelt[2*], Ralf Ebinghaus[2], Johannes Bieser[2], Carl A.M.

7   Brenninkmeijer[1], Armin Rauthe-Schöch[1§], Markus Hermann[3], Bengt G. Martinsson[4],

8   Peter van Velthoven[5], Harald Bönisch[6], Marco Neumaier[6], Andreas Zahn[6], Helmut

9   Ziereis[7]

11   [1]Max-Planck-Institut für Chemie (MPI), Air Chemistry Division, Hahn-Meitner-Weg 1,

12   D-55128 Mainz, Germany

13   [2]Helmholtz-Zentrum Geesthacht (HZG), Institute of Coastal Research, Max-Planck-Str.

14   1, D-21502 Geesthacht, Germany

15   [3]Leibniz-Institut für Troposphärenforschung (Tropos), Permoserstr. 15, D-04318 Leipzig,

16   Germany

17   [4]University of Lund, Division of Nuclear Physics, P.O. Box 118, S-22100 Lund, Sweden

18   [5]Royal Netherlands Meteorological Institute (KNMI), P.O.Box 201, NL-3730 AE, de

19   Bilt, the Netherlands

20   [6]Institute of Meteorology and Climate Research (IMK), Karlsruhe Institute of

21   Technology, Hermann-von-Helmholtz-Platz, D-76344 Eggenstein-Leopoldshafen

22   [7]Deutsches Zentrum für Luft- und Raumfahrt (DLR), Institut für Physik der Atmosphäre,

23   D-82230 Wessling, Germany

25   *now with Bundesamt für Seeschifffahrt und Hydrographie (BSH), Wüstland 2, D-22589

26   Hamburg, Germany

27   §now with Deutscher Wetterdienst, Global Precipitation Climatology Centre, Frankfurter

28   Straße 135, 63067 Offenbach/Main, Germany

30   *Correspondence to:* franz.slemr@mpic.de

32   **Abstract**

34   Mercury was measured onboard the IAGOS-CARIBIC passenger aircraft since May 2005

35   until February 2016 during nearly monthly sequences of mostly four intercontinental

36   flights from Germany to destinations in North and South America, Africa, and South and

37   East Asia. Most of these mercury data were obtained using an internal default signal

38   integration procedure of the Tekran instrument but since April 2014 more precise and

39   accurate data were obtained using post-flight manual integration of the instrument raw

40   signal. In this paper we use the latter data.

41

42   Elevated upper tropospheric total mercury (TM) concentrations due to large scale

43   biomass burning were observed in the upper troposphere (UT) at the equator and

44   southern latitudes during the flights to Latin America and South Africa in boreal autumn

45   (SON) and boreal winter (DJF). TM concentrations in the lowermost stratosphere (LMS)

46   decrease with altitude above the thermal tropopause but the gradient is less steep than

47   reported before. Seasonal variation of the vertical TM distribution in the UT and LMS is

48   similar to that of other trace gases with surface sources and stratospheric sinks. Using

49   speciation experiments, we show that nearly identical TM and gaseous elementary

50   mercury (GEM) concentrations exist at and below the tropopause. Above the thermal

51   tropopause GEM concentrations are almost always smaller than those of TM and the TM

52   – GEM (i.e. Hg^{2+}) difference increases up to ~40% of TM at ~2 km and more above the

53   thermal tropopause. Correlations with N_2O as a reference tracer suggest stratospheric

54   lifetimes of 72 ± 37 and 74 ± 27 yr for TM and GEM, respectively, comparable to the

55   stratospheric lifetime of COS. This coincidence, combined with pieces of evidence from

56   us and other researchers, corroborates the hypothesis that Hg^{2+} formed by oxidation in the

57   stratosphere attaches to sulfate particles formed mainly by oxidation of COS and is

58   removed with them from the stratosphere by air mass exchange, gravitational

59   sedimentation, and cloud scavenging processes.

60

61   **1 Introduction**

62

63   Mercury is a heavy metal whose high vapor pressure leads to significant emissions into

64   the atmosphere. Moreover, due to its slow rate of oxidation and low solubility in water it

65   can be transported over long distances. After oxidation to less volatile and more soluble

66   compounds, mercury is thus deposited in remote areas. Its conversion to the highly

67   neurotoxic methyl mercury which bioaccumulates in the aquatic nutritional chain to

68   concentrations dangerous for humans and animals has motivated intensive research on

69   the biogeochemical cycle of mercury (e.g. Mergler et al., 2007; Scheuhammer et al.,

70   2007; Lindberg et al., 2007, AMAP/UNEP, 2013 and references therein).

71

72   Despite decades of research, the atmospheric mercury cycle is still not well understood

73   (Lin et al., 2006; Lindberg et al., 2007, Ariya et al., 2015). Several mechanisms of

74   elemental mercury oxidation in the gas phase have been proposed (Selin et al., 2007;

75   Holmes et al., 2010; Dibble et al., 2012; Horowitz et al., 2017, Travnikov et al., 2017) but

76   their relative importance is still unknown (Lin et al., 2006; Travnikov et al., 2017).

77   Neither have the oxidation products been unequivocally identified so far because of the

78   lack of speciation techniques for individual mercury compounds (Gustin et al., 2015;

79   Ariya et al., 2015). In addition, attempts to constrain the atmospheric mercury cycle using

80   different models had to rely almost exclusively on measurements at the surface in the

81   northern hemisphere, which undermined these efforts. Measurements of mercury

82   distribution in the troposphere and stratosphere by research aircraft are expensive and

83   thus usually limited to short-term campaigns covering small regions of the globe

84   (Ebinghaus and Slemr, 2000; Friedli et al., 2001, 2003a and 2004; Banic et al., 2003;

85   Ebinghaus et al., 2007; Radke et al., 2007, Talbot et al., 2007a and b, Swartzendruber et

86   al., 2008; Slemr et al., 2009; Lyman and Jaffe, 2012; Brooks et al., 2014, Slemr et al.,

87   2014; Ambrose et al., 2015; Gratz et al., 2015; Weigelt et al., 2016a and b). These

88   measurements have so far provided information about the emissions of mercury from

89   biomass burning (Friedli et al., 2001, 2003a and b; Ebinghaus et al., 2007) and from

90   industrial sources (Friedli et al., 2004; Talbot et al., 2007b; Swartzendruber et al., 2008,

91   Slemr, et al., 2014; Ambrose et al., 2015; Weigelt et al., 2016b), with sometimes

92   conflicting information about the vertical distribution of mercury (Ebinghaus and Slemr,

93   2000; Radke et al., 2007; Talbot et al., 2007a and b; Slemr et al., 2009; Lyman and Jaffe,

94   2012; Brooks et al., 2014; Weigelt et al., 2016a; Bieser et al., 2017). In addition, a

95   pronounced depletion of elemental mercury in air masses influenced by the stratosphere

96   has been reported (Ebinghaus et al., 2007; Radke et al., 2007; Talbot et al., 2007a and b,

97   Swartzendruber et al., 2008, Slemr et al., 2009; Lyman and Jaffe., 2012). Because of

98   temporal and spatial limitations resulting from the costs of research aircraft hardly any

99   information on seasonal variation of mercury concentrations in the upper troposphere

100 (UT) and lowermost stratosphere (LMS) have been obtained so far.

101

102 IAGOS-CARIBIC (*In*-service *A*ircraft for a *G*lobal *O*bserving *S*ystem - *C*ivil *A*ircraft for

103 *R*egular *I*nvestigation of the Atmosphere *B*ased on an *I*nstrumented *C*ontainer) project

104 offers a possibility of regular large scale sounding of trace gas distributions in the UT/LS

105 using an instrumented container flown onboard a passenger aircraft during

106 intercontinental flights (Brenninkmeijer et al., 2007, www.caribic-atmospheric.com).

107 From May 2005 until February 2016 mercury was measured with a modified Tekran

108 instrument in combination with a large suite of other trace gases and particles onboard the

109 CARIBIC aircraft (Brenninkmeijer et al., 2007, Slemr et al., 2009, 2014, 2016). The

110 mercury data collected during nearly monthly sequences of mostly four intercontinental

111 flights from Germany to destinations in North and South America, Africa, and East and

112 South Asia represent the largest mercury data set obtained in the UT and LMS so far.

113 Most mercury data were obtained using the Tekran internal default signal integration

114 procedure but since April 2014 we manually integrated the Tekran raw signal after the

115 flights. The post-flight integration of the raw signal substantially improved the detection

116 limit and precision of the mercury measurements and removed negative bias of the

117 default integration leading to occasional occurrence of zero concentrations in the data

118 before April 2014 (Slemr et al., 2016; Ambrose, 2017). Raw signal data are available

119 only since April 2014 and older data cannot be reintegrated. We use here the recent,

120 smaller but higher quality dataset, to figure out the fate of mercury in the lowermost

121 stratosphere.

122

123 **2 Experimental**

124

125   The CARIBIC container (Brenninkmeijer et al., 2007; www.caribic-atmospheric.com)

126   onboard an Airbus 340-600 of Lufthansa holds automated analyzers for gaseous mercury,

127   CO, O_3, NO, NOy, CO_2, CH_4, acetone, acetonitrile, water vapor (total, gaseous, isotope

128   composition), and fine aerosol particles (three counters for particles with lower threshold

129   diameters of 4 nm, 12 nm, and 18 nm, upper cut off about 2.0 μm), as well as an optical

130   particle size spectrometer (OPSS) for particles with diameters > 150 nm. In addition,

131   whole air and aerosol particle samples are taken in flight and subsequently analyzed for

132   greenhouse gases, halocarbons, hydrocarbons, and particle elemental composition. The

133   CARIBIC measurement container is usually deployed monthly during a sequence of four

134   intercontinental flights.

135

136   The air inlet system and the mercury instrument are described in detail by

137   Brenninkmeijer et al. (2007) and Slemr et al. (2016), respectively. Briefly, the trace gas

138   inlet consists of a trace gas diffuser tube with a flow of more than 2000 volume-l min^{-1}

139   from which ~80 volume-l min^{-1} is taken at a right angle to a manifold which supplies the

140   trace gas analyzers in the container via a temperature controlled PFA lined supply line.

141   The large air velocity in the trace gas diffuser tube and perpendicular sampling at much

142   smaller velocity discriminate against particles larger than about one micrometer diameter

143   (~50% aspiration efficiency, Baron and Willeke, 2001). A modified Tekran instrument

144   (Tekran-Analyzer Model 2537 A, Tekran Inc., Toronto, Canada) samples 0.5 l (STP, i.e.

145   1013.25 hPa and 273.15 K) min^{-1} of air from the supply line manifold (heated to 40°C)

146   using the 4 mm ID PFA tubing at about 30°C. The major modifications of the instrument

147   were the addition of a second pump supporting the internal Tekran pump and of a

148   computer which communicates with the container master computer and controls the

149   automatic operation of the instrument. For the period August 2014 until February 2016 a

150   quartz wool scrubber was installed in the instrument to filter out gaseous oxidized

151   mercury (GOM).

152

153   To achieve an improved spatial resolution of ~ 75 km, the instrument was run with a

154   sampling time of only 5 min. Despite an additional pump the nominal flow of 0.5 l (STP)

155   min^{-1} could not be sustained at the highest flight levels. Limited air flow, the short

156   sampling time, and low concentrations resulted in only ~2 pg of mercury which is much

157   smaller than 10 pg considered as minimum for bias-free internal default integration of the

158   signal by the Tekran instrument (Swartzendruber et al., 2009; Slemr et al., 2016;

159   Ambrose, 2017). The raw analyzer signals were thus processed post flight using a manual

160   integration procedure described in detail by Slemr et al. (2016). The detection limit and

161   precision with post-flight processing is estimated to be ~0.05 ng m^{-3}. The instrument is

162   calibrated after every second flight sequence by comparison with a calibrated reference

163   Tekran instrument in the laboratory. All concentrations are reported in ng Hg m^{-3}(STP).

164

165   As discussed in detail by Slemr et al. (2016) we can assume that our measurements

166   encompass gaseous elemental mercury (GEM), gaseous oxidized mercury (GOM), and

167   about 70% of particle bound mercury (PBM). Speciation experiments with soda lime and

168   KCl coated quartz sand as GOM scrubbers made during several flights demonstrated that

169   GOM passes through the CARIBIC sampling system. According to the extrapolation of

170   the reported GOM/PBM (GOM and PBM are both assumed to be Hg^{2+}, i.e. PBM + GOM

171   = Hg^{2+}) partitioning equilibria (Rutter and Schauer, 2007; Amos et al., 2012) from

172   ambient temperatures near ground to ~ -50°C around the tropopause, most of Hg^{2+} will

173   be attached to particles. Although the CARIBIC trace gas inlet is not optimized to collect

174   particles, we estimated that particles with diameter of < 0.5 μm will pass through it,

175   representing ~70% of the aerosol mass. Despite of significant PBM concentrations in the

176   stratosphere reported by Murphy et al. (1998, 2006), we were not able to detect mercury

177   in aerosol samples collected by the CARIBIC impactor sampler downstream of the inlet

178   optimized for quantitative particle sampling. Although not equipped with heaters, the air

179   carrying particles will warm up to ~ +30° on the way from the aerosol inlet to the

180   impactor. Our inability to detect mercury in particle samples thus suggests that Hg^{2+} on

181   particles evaporates when the air sample is heated to ~ +30°C in the inlet tubing and

182   forms GOM. In summary, we assume that our measurements are close to total mercury

183   (TM = GEM + Hg^{2+} = GEM + GOM + PBM) concentration and we refer to them as such.

184

185   In order to get information about the GOM fraction, sample air was passed through a

186   quartz wool scrubber (Lyman and Jaffe, 2012) during the outbound flights between

187   August 2014 and February 2016. Quartz wool GOM scrubbers are claimed not to be

188   influenced by ozone (Ambrose et al., 2013 and 2015) but can release GOM in humid air.

189   Thus high UT/LMS ozone levels pose no problem and humidity effects are likely small

190   or absent. The data collected with quartz wool scrubber are referred here as GEM.

191   However, during half of the flights with quartz wool scrubber GEM concentrations were

192   significantly higher than those of TM during the return flight at the beginning of the

193   flight and the difference decreased during the flights indicating contamination of

194   unknown origin. These data were eliminated from the data set. We note that the tracks

195   and altitudes of the outbound and return flights differ sometimes substantially, especially

196   in the case of the flights to North America (the flight tracks from Germany to North

197   America tend to be substantially further north than those of the return flights). The TM

198   and GEM data are thus not directly comparable even if they were measured on the same

199   day.

200

201   The data reported here were obtained during flights between April 2014 and February

202   2016 whose tracks are shown in Figure 1. All but one monthly flight sequences consisted

203   of four individual intercontinental flights. The altitude of these flights varies typically

204   from ~ 9 km at the beginning of the flight to 11 - 12 km at the end before the final

205   descent. In addition to the meteorological data provided by the aircraft, meteorological

206   parameters along the flight track were calculated from the ECMWF (European Centre for

207   Medium Range Weather Forecasts) data (6-hourly, 60 model levels until February 2006

208   and 90 model levels thereafter, $1^\circ \times 1^\circ$ horizontal resolution). Eight day backward, 3-D

209   kinematic trajectories were calculated with the KNMI model TRAJKS (Scheele et al.,

210   1996, http://projects.knmi.nl/campaign_support/CARIBIC/) at one minute intervals along

211   the flight path. Consequently, 5 trajectories were available for each mercury

212   measurement. The data set consists of 33 and 17 individual flights with valid TM and

213   GEM data, respectively.

214

215   For the data evaluation, the complementary continuous meteorological and chemical data

216   were averaged over the sampling intervals of mercury measurements.

217

218 **3 Results and discussion**

219

220 3.1 Latitudinal TM distribution in the upper troposphere

221

222 Figure 2 shows latitudinal distribution of TM in the upper troposphere (defined as TM

223 concentrations at potential vorticity (PV) of $-1.5 \leq PV \leq 1.5$ PVU, 1 PVU = 10^{-6} K m^2 kg$^-$

224 ^{1} s^{-1}) observed during the flights to South America (Bogota, São Paulo, and Rio de

225 Janeiro) in boreal summer (only July and August), fall (September, October, November),

226 and winter (December, January, February). Corresponding latitudinal distributions of

227 acetonitrile (AN), originating almost solely from biomass burning, and of CO and CH$_4$

228 with large emissions from biomass burning (Andreae and Merlet, 2001) are also shown.

229 The lowest TM concentrations are observed in the latitude bands of 10 – 20°S and 20 -

230 30°S in summer (JA) and the same applies for CO, CH$_4$, and acetonitrile. The highest TM

231 concentrations in 20-30°S latitude band are observed in fall (SON) and the TM

232 concentrations decrease in winter (DJF) as do the CO and acetonitrile mixing ratios in the

233 10 – 20°S latitude band. The highest CO and CH$_4$ mixing ratios at 20 – 30°S are observed

234 in winter with mixing ratios in fall somewhat lower. Biomass burning in South America

235 starts in June, peaks in September and ends in December (Duncan et al., 2003). TM

236 concentrations in the southernmost latitude bands follow this seasonal variability as do

237 the acetonitrile, CO and CH$_4$ mixing ratios at 10 – 20°S latitude. In the latitude band 20 –

238 30°S the CO and CH$_4$ mixing ratios are higher in boreal winter than in fall. This might

239 result from larger additional CO and CH$_4$ sources in boreal winter such as from oxidation

240 of volatile organic compounds and wetlands. It is also worth noting that in boreal fall and

241 boreal winter the acetonitrile and CO mixing ratios in the monitored part of the southern

242 hemisphere are higher than in the northern hemisphere. In summary, Figure 2 illustrates

243 the large-scale influence of biomass burning on the latitudinal TM distribution in the

244 upper troposphere of the southern hemisphere.

245

246 The role of biomass burning is further illustrated by means of Figure 3, comparing the

247 South America boreal winter profiles of the four trace constituents with those for South

248 Africa (Cape Town). Acetonitrile and CO mixing ratios from flights to South Africa

249   show a pronounced bulge between 30°S and 20°N peaking around the equator. The same

250   applies to results for the flights to South America, be it with somewhat lower values and

251   more southern maximum for acetonitrile. For both flight routes CO and acetonitrile

252   mixing ratios are higher in the southern than in the northern hemisphere. Boreal winter

253   (DJF) is an intermediate season between biomass emissions peaking in September in

254   southern Africa and in January in northern Africa (Duncan et al., 2003). The latitudinal

255   pattern of CH_4 is less clear, with wetlands also being a major source. Finally, Figure 3

256   shows a similarity between TM and the biomass burning indicators in the tropics at flight

257   altitude.

258

259   Biomass burning plumes with enhanced mercury concentrations have been reported

260   before (Brunke et al., 2001; Friedli et al., 2001, 2003a and b, Ebinghaus et al., 2007,

261   Slemr et al., 2014, among others). With 675 Mg yr^{-1} biomass burning is estimated to be

262   the third largest source of atmospheric mercury after emissions from oceans (2682 Mg yr^{-1}

263   ) and from fossil-fuel power plants (810 Mg yr^{-1}; Friedli et al., 2009; Pirrone et al.,

264   2010). Figures 2 and 3 illustrate the influence of biomass burning on the large scale

265   distribution of TM in the southern hemispheric UT.

266

267   Acetonitrile mixing ratios in winter (DJF) in Figure 3 are the lowest in the northernmost

268   latitude bands 20 – 50°N. The concomitant elevated TM concentrations and CO and CH_4

269   mixing ratios are thus mostly due to anthropogenic emissions. An exception is the highest

270   TM concentration observed at 30 – 40°N (Figure 2) in summer (JA) which coincides with

271   the peak of acetonitrile mixing ratio in the northern hemisphere. The respective data

272   originate from the flight #475 from São Paulo to Munich on August 21, 2014. Two whole

273   air samples were taken within this latitude band of which sample #12 coincides with the

274   peak acetonitrile, acetone, CO, and CH_4 mixing ratios. In addition, sample #12 contains

275   high ethane and propane mixing ratios (786 and 126 ppt, respectively) as well as

276   somewhat elevated CH_4 and SF_6 mixing ratios. Sample #12 was taken over southwestern

277   Spain and its 8 day backward trajectory crosses the Atlantic Ocean, eastern US, Great

278   Lakes up to Californian Pacific coast. The complex composition of this sample indicates

279   a mixture of anthropogenic pollution with emissions from biomass burning. The latter is

280 additionally   supported   by   fire   maps

281 (https://lance.modaps.eosdis.nasa.gov/imagery/firemaps) reporting individual fire counts

282 along the trajectory in North America and especially a large fire in northern California at

283 the time of trajectory crossing.

284

285 3.2 Seasonal variation of the vertical TM distribution in the upper troposphere and

286 lowermost stratosphere

287

288 Due to the geographical location of the airport of departure and the CARIBIC

289 destinations it happens to be that half of the intersected air masses are above the

290 tropopause. This allows a fairly representative mapping of measured trace species around

291 the tropopause. Figure 4 shows the seasonal pattern of the average TM concentrations

292 and CO, CH_4, and O_3 mixing ratios relative to the thermal tropopause. The distance

293 relative to the tropopause is based on CARIBIC ozone measurements. Basically, an

294 ozone mixing ratio measured by CARIBIC is compared to representative data from ozone

295 soundings. Because these soundings measure both thermal tropopause height and ozone,

296 the distance relative to the tropopause is obtained (Sprung and Zahn, 2010). This value

297 based on the CARIBIC ozone data is considered to be more accurate than PV (calculated

298 from the ECMWF-model) based dynamical tropopause, especially in subtropical latitudes

299 where the dynamical tropopause is not well defined by a constant PV threshold value

300 (Kunz et al., 2011). Only measurements north of 20°N were considered for making this

301 plot. The seasonal variation of the vertical distributions of the trace gases and TM reflect

302 their source location and the Brewer-Dobson circulation with a maximum content of

303 stratospheric air in the UT/LMS in spring (Holton et al., 1995; Gettelman et al., 2014).

304 Ozone rich air, depleted in CO, CH_4, and N_2O descends in spring and the question is

305 what happens to the mercury compounds.

306

307 The highest tropospheric TM concentrations of $1.4 - 1.7$ ng m^{-3} are encountered in

308 September/October at $0.5 - 1.75$ km below the thermal tropopause. About two thirds of

309 these elevated TM data originate from flights from Tokio to Munich on October 30,

310 2014, and Beijing to Munich on October 31, 2014, and were observed mostly within

311   ~1500 km of Tokio and Beijing. High TM concentrations are accompanied by elevated

312   CO and CH_4 mixing ratios. Near Tokio and Beijing also elevated SF_6 mixing ratios were

313   observed. Backward trajectories from these flight segments on October 30 and 31 point to

314   surface contact in Tibet, Bangladesh, and northern India. Slightly elevated TM

315   concentrations encountered near Munich on October 30 and 31 are most likely due

316   emissions located in North America.

317

318   The lowest TM concentrations of 0.4 – 0.6 ng m^{-3} were encountered during the flights

319   Tokio to Munich (CARIBIC #502) on April 21, 2015, and Mexico to Munich (CARIBIC

320   #504) on April 22, 2015. During both flights the lowest TM concentrations were

321   accompanied by O_3 and H_2O mixing ratios of > 400 ppb and < 10 ppm, respectively,

322   characteristic of deeper stratospheric air. No CO data are available for the CARIBIC

323   flight #502 but CO mixing ratios of < 30 ppb for the lowest TM values during the

324   CARIBIC flight #504 also point to deep stratospheric origin of the air, as confirmed by

325   the extremely low SF_6 and CH_4 mixing ratios in both flights.

326

327   3.3 Speciation in the UT and LMS

328

329   The reason to show only TM in Figure 4, and not GEM as well is that speciation failed

330   for about half of the data due to contamination problems with the quartz wool GOM

331   scrubber. For analyzing the GEM results, we divide the data set into boreal winter

332   (December – May) and boreal summer (June – November). Figure 5 give the vertical

333   distributions of TM and GEM in three different latitude bands for boreal winter (Figure

334   5a) and summer (Figure 5b). The data points in these figures represent concentration

335   averages and their standard errors. Although extreme individual values were eliminated

336   using the Nalimov outlier test (Kaiser and Gottschalk, 1972), unedited data give very

337   similar plots. We also note that TM and GEM data from all flights were used in these

338   figures, altogether 1528 and 1349 TM measurements in winter and summer, respectively,

339   as well 699 and 916 GEM measurements in winter and summer, respectively. As already

340   mentioned GEM data were collected during the outward and TM data during the return

341   flights. Because of different flight tracks and flight altitudes the GEM and TM data

342   cannot be directly compared even if measured on the same day. In addition, because of

343   contamination problems valid GEM data are available only for about one half of the

344   flights with TM data.

345

346   Winter vertical distribution in Figure 5a shows for 30 – 60°N a steep gradient of TM

347   concentrations across the thermal tropopause from ~ 1.25 ng m^{-3} in the UT to ~ 0.6 ng m^{-}

348   ^{3} in the LMS. This gradient corresponds to the steep gradient of TM concentrations in

349   January – May shown in Figure 4. The GEM gradient is steeper starting with

350   concentrations of ~ 1.35 ng m^{-3} and decreasing to concentrations of ~ 0.35 ng m^{-3} in the

351   LMS. The difference between TM and GEM concentrations at altitudes starting at 1 km

352   above the tropopause is ~ 0.2 ng m^{-3} , representing ~ 40% of TM concentration.

353

354   TM and GEM data between 30°S – 30°N cover essentially only the UT because the

355   aircraft cruising altitude of 10 – 12 km is not sufficient to enter the tropical stratosphere.

356   TM and GEM concentrations are essentially the same, but with ~1.2 ng m^{-3} somewhat

357   lower than in the UT at 30 – 60°N where most of the anthropogenic mercury sources are

358   located.

359

360   In the northernmost latitude band (> 60°N) there are few UT data because the aircraft

361   cruising altitude of 10 – 12 km has most of the time been above the tropopause. Starting

362   at altitudes of 1 km above the tropopause, the TM concentrations around ~ 0.6 ng m^{-3} are

363   only slightly higher than GEM concentrations of 0.5 ng m^{-3}. Larger difference between

364   TM and GEM concentrations is observed only at the three highest altitudes above the

365   tropopause.

366

367   Figure 5b shows the summer data which are generally higher than the winter data. In the

368   tropical UT (30°S – 30°N GEM concentrations are with ~ 1.2 ng m^{-3} somewhat lower

369   than those of TM, but the difference is probably insignificant. In the northern

370   midlatitudes the GEM concentrations measured in the UT are higher than TM This is not

371   a contradiction because of the different tracks of outbound (GEM measurements) and

372   return (TM measurements) flights to North America and different influence of biomass

373   burning on particular flights. It appears that in the LMS the differences are small.

374

375   At mid latitudes and north of 60°N, TM gradients around the tropopause are much less

376   steep in summer than in winter (Figure 5a), which is consistent with the seasonal

377   variation of TM concentrations in UT/LMS shown in Figure 4. There is not much

378   difference between TM and GEM concentrations in the midlatitude LMS, but at >60°N at

379   2 – 3 km above the tropopause GEM concentrations with ~ 0.6 ng m^{-3} are consistently

380   lower than those of TM with ~0.8 ng m^{-3}.

381

382   In summary, TM concentrations are lowest (with ~ 0.5 ng m^{-3}) in stratosphere at the

383   highest altitude above the tropopause (3 – 4 km). GEM concentrations are comparable to

384   those of TM in the UT, but systematically smaller in the LMS at middle latitude in winter

385   and at northernmost latitudes in summer.

386

387   Our notion about the behavior and speciation of mercury in the UT/LMS is quite limited

388   and based on a few measurement reports. Swartzendruber et al. (2006) observed at Mount

389   Bachelor higher GOM concentration in downslope air flow than in upslope flow which

390   implies higher GOM concentrations in the free troposphere than in the planetary

391   boundary layer. Talbot et al. (2007a) reported a total depletion of GEM in the UT/LMS.

392   By extrapolation of measurements in stratospheric intrusions, Lyman and Jaffe (2012)

393   derived an empirical model which predicts a total depletion of GEM at ~ 1 km above the

394   tropopause and of total mercury (including particle bond mercury, PBM) at some 2 km

395   above the tropopause. The latter is inconsistent with observations of substantial PBM

396   concentrations in the stratosphere up to an altitude of 8 km above the tropopause reported

397   by Murphy et al. (1998, 2006). Brooks et al. (2014) reported decreasing GOM

398   concentrations above GOM maxima at ~ 4 km altitude above ground. They also found

399   that GEM concentrations are independent of altitude between ground and 6 km altitude

400   for most of the year. Only in April, May and June GEM concentrations decreased with

401   increasing altitude possibly because of the intensive influx of stratospheric air in this

402   season. Gratz et al. (2015) observed in June 2013 high GOM concentrations in

403   tropospheric air mass rich in BrO advected from the subtropical Pacific.

404

405   Opposite to the total GEM depletion reported by Talbot et al. (2007a) and predictions by

406   Lyman and Jaffe (2012) our post-flight processed GEM and TM concentrations were

407   never below the detection limit of ~0.05 ng m^{-3}, even at 4 km altitude above the

408   tropopause. However, when using the default Tekran software, small mercury peaks are

409   occasionally not integrated resulting in erroneous zero concentrations. We thus surmise

410   that the zero GEM concentrations reported by Talbot et al. (2007a) were not real but an

411   artifact due to incorrect default integration of the Tekran raw signal (Swartzendruber et

412   al., 2009; Slemr et al., 2016; Ambrose, 2017). We also note that Talbot et al. (2007a)

413   attribute their measurements to GEM although their inlet system is very similar to that of

414   CARIBIC (Slemr et al., 2014) with proven transmission of GOM. As for CARIBIC, the

415   measurements by Talbot et al. (2007a) are thus more likely close to those of TM.

416

417   Based on TM and GEM measurements outside of a stratospheric intrusion, Lyman and

418   Jaffe (2012) found Hg^{2+} (GOM + PBM = TM - GEM) to be dominant mercury species at

419   the tropopause. By extrapolation of the data using empirical correlations of TM and Hg2+

420   with ozone, they predicted zero TM concentrations already at ~ 2 km above the

421   tropopause and speculated that this may generally apply for the UT/LMS. This is

422   inconsistent with our measurements that show comparable GEM and TM concentrations

423   in the UT with Hg^{2+} constituting at most ~ 50% of TM up to 4 km above the tropopause.

424   It is also inconsistent with regular vertical profiling of GEM, GOM, and PBM up to 6 km

425   altitude above ground by Brooks et al. (2014). They report tropospheric GOM maxima of

426   up to ~ 0.11 ng m^{-3} at ~ 4 km above ground and decreasing GOM concentrations above.

427   Elevated Hg^{2+} concentrations in the UT during the NOMADDS (Nitrogen, Oxidants,

428   Mercury and Aerosol Distributions, Sources and Sinks) campaign were reported by Gratz

429   et al. (2015) but only for an advected tropospheric air mass with high BrO content (Gratz

430   et al., 2015). We thus conclude that high GOM concentrations in the UT reported by

431   Lyman and Jaffe (2012) are most likely an event phenomenon which cannot be

432   generalized.

433

434   Zero TM concentrations at ~ 2 km above the tropopause from the empirical model of

435   Lyman and Jaffe (2012) are, in addition, not conform to the observations of significant

436   PBM concentrations in stratosphere by Murphy et al. (1998, 2006). Gaseous Hg^{2+} (GOM)

437   is assumed to be in equilibrium with PBM. An extrapolation of the equilibria observed at

438   ambient air temperatures near ground (Rutter and Schauer, 2007; Amos et al., 2012) to

439   some -50°C around the tropopause shows that almost all Hg^{2+} will be on particles.

440   Substantial PBM concentrations observed by Murphy et al. (1998, 2006) up to 8 km

441   above the tropopause together with our TM data obtained during some 500 CARIBIC

442   flights (including those with default Tekran raw signal integration) thus exclude the

443   possibility that TM disappears at ~ 2 km above the tropopause. We also note that Murphy

444   et al. (1998, 2006) could not detect any PBM in the troposphere at and below 5 km above

445   ground. Non-detectable PBM in equilibrium with GOM at still low air temperatures at

446   these altitudes is another piece of evidence inconsistent with generally high GOM

447   concentrations in the upper free troposphere.

448

449   In summary, it is plausible that our TM data currently provide the most representative

450   picture of its UT/LS distribution and seasonal variation. Our GEM measurements rely on

451   the performance of the GOM quartz wool traps and the difference between TM and GEM

452   is statistically compromised by not being measured along exactly the same routes and

453   altitudes above the tropopause. Despite this, our TM and GEM observations suggest only

454   a small contribution of Hg^{2+} to TM in the UT and are consistent with the observations of

455   substantial PBM concentrations in UT/LS by Murphy et al. (1998, 2006).

456

457   3.4 Stratospheric lifetime of TM and GEM

458

459   N_2O and SF_6 measured in the whole air samples taken during the CARIBIC flights can be

460   used as chronological tracers to estimate the stratospheric lifetime of TM and GEM. Here

461   we use the relative approach described by Volk et al. (1997) using the CARIBIC N_2O

462   measurements (Assonov et al., 2013) as reference tracer. N_2O, with a lifetime of ~120 yr

463   is nearly uniformly distributed in the troposphere, with little seasonal variation and is

464   only removed in the stratosphere (Nevison et al., 2011). In comparison with SF_6 as

465   chronological tracer, N_2O has the advantage of a much smaller latitudinal gradient in the

466   troposphere and of nearly constant growth rate in the last two decades. Figure 6 shows

467   winter (November – April) average stratospheric TM and GEM concentrations as a

468   function of N_2O mixing ratios. In this plot N_2O mixing ratios were detrended using 2015

469   as a reference year and the N_2O growth rate of 0.844 ppb yr^{-1} (Assonov et al., 2013).

470

471   TM and GEM concentrations in Figure 6 start at 1.18 ± 0.27 (n = 48) and 1.12 ± 0.21 (n =

472   35) ng m^{-3}, respectively, in the 325 – 330 ppb bin of N_2O mixing ratios and they decrease

473   substantially to 0.59 ± 0.13 (n = 12) and 0.42 ± 0.10 (n = 16) ng m^{-3}, respectively, in the

474   305 – 310 ppb bin. The difference between TM and GEM concentrations is not

475   statistically significant in the 325 – 330 ppb bin of N_2O mixing ratios, i.e. in the UT as

476   already mentioned before. At lower N_2O mixing ratios, however, GEM concentrations

477   are systematically smaller than those of TM at the 99% significance level. The TM-GEM

478   difference (i.e. Hg^{2+} concentration in the gas phase (GOM) and on particles (PBM)) is

479   increasing with decreasing N_2O mixing ratios and levels off at ~ 0.17 ng m^{-3} at N_2O

480   mixing ratios below 315 ppb representing ~ 30% of TM concentrations. As mentioned in

481   the experimental section, the CARIBIC trace gas inlet is not optimized for quantitative

482   collection of particles and, consequently, we presume to measure only ~ 70% of Hg^{2+} on

483   particles. If all Hg^{2+} (i.e. TM-GEM) were on particles as predicted by extrapolation of

484   Hg^{2+} gas-particle partitioning equilibrium (Rutter and Schauer, 2007; Amos et al., 2012)

485   from ambient temperature to temperatures at the tropopause then the unbiased Hg^{2+} and

486   TM concentrations would be ~ 0.24 and ~ 0.66 ng m^{-3}, respectively, at N_2O mixing ratios

487   below 310 ppb.

488

489   Small decrease of TM and GEM with decreasing N_2O below 315 ppb suggests a long

490   stratospheric lifetime of both TM and GEM. Correlations of all TM and GEM

491   concentrations at N_2O mixing ratios < 315 ppb vs N_2O yield slopes of 6.30 ± 2.96 pg m^{-3}

492   ppb^{-1} (n = 46, R = 0.2947, significance > 95%) and 6.13 ± 1.82 pg m^{-3} ppb^{-1} (n = 63, R =

493   0.3909, significance > 99%), for TM and GEM, respectively. Using stratospheric N_2O

494   lifetime of 122 ± 24 yr (Volk et al., 1997) we arrive at stratospheric TM and GEM

495   lifetimes of 72 ± 37 and 74 ± 27 yr, respectively. The uncertainties calculated from the

496   slope uncertainties and the uncertainty of N_2O lifetime are probably lower limit because

497   of the narrow range of encountered N_2O mixing ratios in cruising altitudes of the

498   CARIBIC aircraft (Assonov et al., 2013). We note that our stratospheric TM and GEM

499   lifetimes are not "relatively short" as claimed by Lyman and Jaffe (2012). We think that

500   their TM and GEM concentrations were measured within the region of mixing of

501   stratospheric with tropospheric air. Figure 6 shows that TM and GEM vs N_2O

502   correlations would result in much shorter lifetimes when data at N_2O mixing ratios larger

503   than 315 ppb were included. With the calculated uncertainties the stratospheric TM

504   lifetime cannot be distinguished from that of GEM. A more precise estimate of TM and

505   GEM stratospheric lifetimes will require measurements with research aircraft capable of

506   flying at higher altitudes.

507

508   Data in Figure 6 allow us to correlate Hg^{2+} (TM - GEM) with GEM as made by Lyman

509   and Jaffe (2012). Hg^{2+} is negatively correlated with GEM with a slope of -0.13 ± 0.04 (n

510   = 7, R^2 = 0.712) and -0.31 ± 0.04 (n = 7, R^2 = 0.919) when averages and medians are

511   used, respectively. Chemical conversion of GEM into Hg^{2+} without any Hg^{2+} losses

512   would yield a slope of -1 and slopes near this value were reported for the free troposphere

513   by Swartzendruber et al. (2006) and for the UT by Lyman and Jaffe (2012). Our negative

514   slopes in the stratosphere are substantially greater than -1 and somewhat greater than -

515   0.53 reported by Lyman and Jaffe (2012) for stratosphere-influenced air masses.

516   Negative slopes greater than -1 imply losses of Hg^{2+} (Hg^{2+} yield of GEM oxidation is

517   smaller than the stoichiometry of the reaction) and result in decreasing TM

518   concentrations with increasing Hg^{2+} concentrations in the stratosphere.

519

520   A reduction of TM concentration from ~ 1.2 ng m^{-3} in tropospheric air to ~ 0.66 ng m^{-3} in

521   stratospheric air is too large to be explained by the aerosol bias induced by the

522   incomplete particle sampling mentioned above and requires Hg^{2+} removal process. Such

523   removal process requires an oxidation of GEM into Hg^{2+}, an attachment of Hg^{2+} to

524   abundant stratospheric, mainly sulfate, particles, and their removal by gravitational

525   sedimentation and/or scavenging by clouds (Menzies and Tratt, 1995; Rasch et al., 2008;

526   Lyman and Jaffe, 2012). We note that air mass exchange is also taking important part in

527   removing the sulfate particles from the stratosphere but TM concentrations would not

528   change without sedimentation and scavenging of Hg^{2+} on particles. The oxidation and

529   subsequent attachment to particles could be a local process in the vicinity of extratropical

530   tropopause layer (exTL) or a non-local process in the tropical upper troposphere (TTL)

531   and during the transport from the TTL to the location of the IAGOS-CARIBIC

532   measurements in the LMS. Lyman and Jaffe (2012) hypothesized that Hg^{2+} formed by

533   GEM oxidation in the TTL and/or stratosphere will attach to sulfate particles formed in

534   the stratosphere predominantly by COS oxidation and be removed with them (Wilson et

535   al., 2008). This hypothesis is corroborated by our stratospheric TM and GEM lifetimes

536   which are comparable to COS lifetime of 64 ± 21 yr (Barkley et al., 2008). As pointed

537   out by Lyman and Jaffe (2102), the hypothetical model of stratospheric mercury is thus

538   similar and closely related to that of stratospheric sulfur (COS + sulfate particles) as

539   described by Wilson et al. (2008).

540

541   **Conclusions and outlook**

542

543   The obvious implication of the long stratospheric TM and GEM lifetimes is that most

544   atmospheric mercury is oxidized in the troposphere. The second direct implication is that

545   if the lifetime of GEM in the stratosphere with its very high O_3 mixing ratios (typically 1

546   ppm and more) is quite long, then the GEM + O_3 reaction cannot be important in the

547   troposphere with its low O_3 mixing ratios. This implies that either the reaction does not

548   take place or that the primary reaction product is instable. Moreover, with very low

549   stratospheric H_2O mixing ratios below 10 ppm, also OH is an unlikely oxidant for GEM

550   in the stratosphere. The most plausible remaining oxidants are Br atoms with a possible

551   contribution of O atoms.

552

553   The regular intercontinental IAGOS-CARIBIC flights provide an insight into the large-

554   scale distribution of TM and GEM in the UT/LMS and its seasonal variation. Post-flights

555   processed data with better accuracy and higher precision reveal a seasonal variation of

556   vertical TM distribution in the UT/LMS which is similar to most of the trace gases with

557   sources in the troposphere, such as CH_4 and CO. Importantly, even at altitudes of up to

558   3.5 km above the thermal tropopause TM concentrations are still ~0.5 ng m^{-3}, one order

559   of magnitude above the instrumental detection limit. We have never observed zero TM or

560   GEM concentrations and attribute earlier reports about them to an insufficiency in the

561   default signal integration of the Tekran instrument.

562

563   Latitudinal TM distribution in the UT during the flights to South America and South

564   Africa were found to be strongly influenced by biomass burning. Although TM and GEM

565   were not measured at the same place and at the same time, the data collectively show that

566   their concentrations in the UT are similar and the Hg^{2+} concentrations are thus usually

567   small. Recent reports on high GOM and Hg^{2+} concentrations in the free troposphere are

568   limited to middle tropospheric altitudes (Brooks et al., 2014), to an event with high BrO

569   concentrations (Gratz et al., 2015) or to a stratospheric intrusion (Lyman and Jaffe, 2012)

570   and are in view of our observational IAGOS-CARIBIC data set most likely not

571   representative for large-scale UT distribution. Larger Hg^{2+} (TM – GEM) concentrations

572   of up to about half of TM concentrations were observed only in the LMS.

573

574   Lower TM concentrations were generally observed in LMS with the pronounced gradient

575   just above the tropopause. We attribute this gradient to mixing of tropospheric air with

576   stratospheric air depleted of mercury. The conservative character of TM measurements

577   implicates a loss process by oxidation to Hg^{2+}, its attachment to particles and their

578   subsequent removal by gravitational sedimentation and/or scavenging by clouds.

579   Substantial stratospheric PBM concentrations reported by Murphy et al. (1998, 2006) and

580   GOM/PBM equilibria (Rutter and Schauer, 2007; Amos et al., 2012) extrapolated to

581   temperatures in the LMS support this hypothesis.

582

583   Correlations of TM and GEM with N_2O as a reference substance show statistically the

584   same TM and GEM concentrations in the UT. In the N_2O range of 330 and 315 ppb TM

585   and GEM concentrations rapidly decrease with decreasing N_2O mixing ratios due to

586   mixing of tropospheric air with stratospheric air depleted of mercury. Below 315 ppb

587   until 295 ppb of N_2O TM and GEM concentrations hardly change. TM and GEM

588   lifetimes of 72 ± 37 and 74 ± 27 yr, respectively, were calculated from correlations of

589   TM and GEM vs N_2O below 315 ppb, albeit with large uncertainties caused by the

590   limited altitude range of commercial airliners and the resulting narrow range of N_2O

591   mixing ratios between 315 and 295 ppb. Measurements of TM, GEM, and N_2O to higher

592   altitudes above the tropopause (i.e. to N_2O mixing ratios substantially below 290 ppb) are

593   needed to better constrain the stratospheric TM and GEM lifetimes.

594

595   Stratospheric lifetimes of TM and GEM are comparable to the COS stratospheric lifetime

596   of 64 ± 21 yr (Barkley et al., 2008), which is in volcanically quiet periods the major

597   precursor of sulfate particles in the stratosphere (Wilson et al., 2008). This coincidence

598   corroborates the hypothesis of Hg^{2+} attachment to sulfate particles and their removal by

599   gravitational sedimentation and scavenging by clouds. This hypothesis, first proposed by

600   Lyman and Jaffe (2012), could be directly tested in future by quantitative measurements

601   of Hg/S ratios on stratospheric particles. Such measurements would also better constrain

602   the mercury fluxes across the tropopause.

603

604   Mercury measurements onboard IAGOS-CARIBIC were stopped in March 2016 and the

605   space of the mercury instrument is now occupied by other instruments. The reason for the

606   termination of the mercury measurements was the feeling that, with the present

607   instrumentation, we will only reproduce the existing data. An improved instrumentation

608   including reliable speciation technique is needed to gain new insights. Any institution

609   capable of providing and maintaining such an instrument is welcomed to participate in

610   future IAGOS-CARIBIC measurements. For details please consult the CARIBIC

611   coordinator Andreas Zahn.

612

613   **Acknowledgements**

614

615   We thank Lufthansa Airlines and Lufthansa Technik for their commitment and support.

616   We also thank Jan Boedewadt from HZG for modifying the Tekran instrument for

617   deployment in the CARIBIC container. The development and operation of the CARIBIC

618   system has been financially supported by the German Ministry of Education and Science

619   (AFO 2000, IAGOS-D), by the European Commission's DGXII Environment RTD 4th

620   and 5th Framework programs, by grants from the Max Planck Society and from Frankfurt

621   Airport.

622

References

AMAP/UNEP: Technical Background Report for the Global Mercury Assessment, 2013, available at AMAP (www.amap.no) and UNEP Chemicals Branch´s (http://www.unep.org/hazardoussubstances/mercury/informationmaterials/reportsandpublications/tabid/3593/default.aspx) websites.

Ambrose, J.L., Lyman, S.N., Huang, J., Gustin, M.S., and Jaffe, D.A.: Fast time resolution oxidized mercury measurements during the Reno Atmospheric Mercury Intercomparison Experiment (RAMIX), Environ. Sci. Technol., 47, 7285-7294, 2013.

Ambrose, J.L., Gratz, L.E., Jaffe, D.A., Campos, T., Flocke, F.M., Knapp, D.J., Stechman, D.M., Stell, M., Weinheimer, A.J., Cantrell, C.A., and Mauldin III, R.L.: Mercury emission ratios from coal-fired power plants in the southeastern United States during NOMADDS, Environ. Sci. Technol., 49, 10389-10397, 2015.

Ambrose, J.L.: Improved methods for signal processing in measurements of mercury by Tekran 2537A and 2537B instruments, Atmos. Meas. Tech. , 10, 5063-5073, 2017.

Amos, H.M., Jacob, D.J., Holmes, C.D., Fisher, J.A., Wang, Q., Yantosca, R.M, Corbitt, E.S., Galarneau, E., Rutter, A.P., Gustin, M.S., Steffen, A., Schauer, J.J., Graydon, J.A., Louis, V.L.St., Talbot, R.W., Edgerton, E.S., Zhang, Y., and Sunderland, E.M.: Gas-particle partitioning of atmospheric Hg(II) and its effect on global mercury deposition, Atmos, Chem. Phys., 12, 591-603, 2012.

Andreae, M.O., and Merlet, P.: Emission of trace gases and aerosols from biomass burning, Global Biogeochem. Cycles, 15, 955-966, 2001.

Ariya, P.A., Amyot, M., Dastoor, A., Deeds, D., Feinberg, A., Kos, G., Poulain, A., Ryjkov, A., Semeniuk, K., Subir, M., and Toyota, K.: Mercury physicochemical and

653   biogeochemical transformation in the atmosphere and at atmospheric interfaces: A review

654   and future direction, Chem. Rev., 115, 3760-3802, 2015.

655

656   Assonov, S.S., Brenninkmeijer, C.A.M., Schuck, T., and Umezawa, T.: N_2O as a tracer of

657   mixing stratospheric and tropospheric air based on CARIBIC data with applications for

658   CO_2, Atmos. Environ., 79, 769-779, 2013.

659

660   Banic, C.M., Beauchamp, S.T., Tordon, R.J., Schroeder, W.H., Steffen, A., Anlauf, K.A.,

661   and Wong, K.H.T.: Vertical distribution of gaseous elemental mercury in Canada, J.

662   Geophys. Res., 108 (D9), 4264, doi:10.1029/2002JD002116, 2003.

663

664   Barkley, M.P., Palmer, P.I., Boone, C.D., Bernath, P.F., and Sunthralanigam, P.: Global

665   distributions of carbonyl sulfide in the upper troposphere and stratosphere, Geophys. Res.

666   Lett., 35, L14810, doi:10.1029/2008GL034270, 2008.

667

668   Baron, P. A., and Willeke K.: Aerosol Measurements: Principles Techniques and

669   Applications, John Wiley and Sons, New York, 1131 pp, 2001.

670

671   Bieser, J., Slemr, F., Ambrose, J., Brenninkmeijer, C., Brooks, S., Dastoor, A.,

672   DeSimone, F., Ebinghaus, R., Gencarelli, C.N., Geyer, B., Gratz, L.E., Hedgecock, I.M.,

673   Jaffe, D., Kelley, P., Lin, C.-J., Jaegle, L., Matthias, V., Ryjkov, A., Selin, N.E., Song, S.,

674   Travnikov, O., Weigelt, A., Luke, W., Ren, X., Zahn, A., Yang, X., Zhu, Y., and Pirrone,

675   N.: Multi-model study of mercury dispersion in the atmosphere: vertical and

676   interhemispheric distribution of mercury species, Atmos. Chem. Phys., 17, 6925-6955,

677   2017.

678

679   Brenninkmeijer, C.A.M., Crutzen, P., Boumard, F., Dauer, T., Dix, B., Ebinghaus, R.,

680   Filippi, D., Fischer, H., Franke, H., Frieß, U., Heintzenberg, J., Helleis, F., Hermann, M.,

681   Kock, H.H., Koeppel, C., Lelieveld, J., Leuenberger, M., Martinsson, B.G., Miemczyk,

682   S., Moret, H.P., Nguyen, H.N., Nyfeler, P., Oram, D., O'Sullivan, D., Penkett, S., Platt,

683   U., Pupek, M., Ramonet, M., Randa, B., Reichelt, M., Rhee, T.S., Rohwer, J., Rosenfeld,

684 K., Scharffe, D., Schlager, H., Schumann, U., Slemr, F., Sprung, D., Stock, P., Thaler, R.,
685 Valentino, F., van Velthoven, P., Waibel, A., Wandel, A., Waschitschek, K.,
686 Wiedensohler, A., Xueref-Remy, I., Zahn, A., Zech, U., and Ziereis, H.: Civil aircraft for
687 the regular investigation of the atmosphere based on an instrumented container: The new
688 CARIBIC system, Atmos. Chem. Phys., 7, 1-24, 2007.

689

690 Brooks, S., Ren, X., Cohen, M., Luke, W.T., Kelley, P., Artz, R., Hynes, A., Landing,
691 W., and Martos, B.: Airborne vertical profiling of mercury speciation near Tullahoma,
692 TN, USA, Atmosphere, 5, 557-574, 2014.

693

694 Brunke, E.-G., Labuschagne, C., and Slemr, F.: Gaseous mercury emissions from a fire in
695 the Cape Peninsula, South Africa, during January 2000, Geophys. Res. Lett., 28, 1483-
696 1486, 2001.

697

698 Dibble, T.S., Zelie, M.J., and Mao, H.: Thermodynamics of reactions of ClHg and BrHg
699 radicals with atmospherically abundant free radicals, Atmos. Chem. Phys., 12, 10271-
700 10279, 2012.

701

702 Duncan, B.R., Martin, R.V., Staudt, A.C., Yevich, R., and Logan, J.A.: Interannual and
703 seasonal variability of biomass burning emissions constrained by satellite observations, J.
704 Geophys. Res., 108, doi: 10.1029/2002JD002378, 2003.

705

706 Ebinghaus, R. and Slemr, F.: Aircraft measurements of atmospheric mercury over
707 southern and eastern Germany, Atmos. Environ., 34, 895-903, 2000.

708

709 Ebinghaus, R., Slemr, F., Brenninkmeijer, C.A.M., van Velthoven, P., Zahn, A.,
710 Hermann, M., O´Sullivan, D.A., and Oram, D.E.: Emissions of gaseous mercury from
711 biomass burning in South America in 2005 observed during CARIBIC flights, Geophys.
712 Res. Lett., 34, L08813, doi:10.1029/2006GL028866, 2007.

713

714 Friedli, H.R., Radke, L.F., and Yu, J.Y.: Mercury in smoke from biomass fires, Geophys.
715 Res. Lett., 28, 3223-3226, 2001.

716

717 Friedli, H.R., Radke, L.F., Lu, J.Y., Banic, C.M., Leaitch, W.R., and MacPherson, J.I.:
718 Mercury emissions from burning of biomass from temperate North American forests:
719 laboratory and airborne measurements, Atmos. Environ., 37, 253-267, 2003a.

720

721 Friedli, H.R., Radke, L.F., Prescott, R., Hobbs, P.V., and Sinha, P.: Mercury emissions
722 from the August 2001 wildfires in Washington State and an agricultural waste fire in
723 Oregon and atmospheric mercury budget estimates, Global Biogeochem. Cycles, 17,
724 doi:10.1029/2002GB001972, 2003b.

725

726 Friedli, H.R., Radke, L.F., Prescott, R., Li, P., Wo, J.-H., and Carmichael, G.R.: Mercury
727 in the atmosphere around Japan, Korea, and China as observed during the 2001 ACE-
728 Asia field campaign: Measurements, distributions, sources, and implications, J. Geophys.
729 Res., 109, D19S25, doi:10.1029/2003JD004244, 2004.

730

731 Friedli, H.R., Arellano, A.F., Cinnirella, S., and Pirrone, N.: Initial estimates of mercury
732 emissions to the atmosphere from global biomass burning, Environ. Sci. Technol., 43,
733 3507-3513, 2009.

734

735 Gettelman, A., Hoor, P., Pan, L.L., Randel, W.J., Hegglin, M.I., and Birner, T.: The
736 extratropical upper troposphere and lower stratosphere, Rev. Geophys., 49, RG3003,
737 doi:10.1029/2011RG000355, 2011.

738

739 Gratz, L.E., Ambrose, J.L., Jaffe, D.A., Shah, V. Jaeglé, L., Stutz, J., Festa, J., Spolaor,
740 M., Tsai, C., Selin, N.E., Song, S., Zhou, X., Weinheimer, A.J., Knapp, D.J., Montzka,
741 D.D., Flocke, F.M., Campos, T.L., Apel, E., Hornbrook, R., Blake, N.J., Hall, S.,
742 Tyndall, G.S., Reeves, M., Stechman, D., and Stell, M.: Oxidation of mercury by
743 bromine in the subtropical Pacific free troposphere, Geophys. Res. Lett., 42,
744 doi:10.1002/2015GL066645, 2015.

745

746   Gustin, M.S., Amos, H.M., Huang, J., Miller, M.B., and Heidecorn, K.: Measuring and

747   modeling mercury in the atmosphere: a critical review, Atmos. Chem. Phys., 15, 5697-

748   5713, 2015.

749

750   Holmes, C.D., Jacob, D.J., Corbitt, E.S., Mao, J., Yang, X., Talbot, R., and Slemr, F.:

751   Global atmospheric model for mercury including oxidation by bromine atoms, Atmos.

752   Chem. Phys., 10, 12037-12057, 2010.

753

754   Holton, J.R., Haynes, P.H., McIntyre, M.E., Douglass, A.R., Rood, R.B., and Pfister, L.:

755   Stratosphere-troposphere exchange, Rev. Geophys., 33, 403-439, 1995.

756

757   Horowitz, H.M., Jacob, D.J., Zhang, Y., Dibble, T.S., Slemr, F., Amos, H.M., Schmidt,

758   J.A., Corbitt, E.S., Marais, E.A., and Sunderland, E.M.: A new mechanism for

759   atmospheric mercury redox chemistry: Implications for the global mercury budget,

760   Atmos. Chem. Phys., 17, 6353-6371, 2017.

761

762   Kaiser, R., and Gottschalk, G.: Elementare Tests zut Beurteilung von Meßdaten,

763   Bibliographisches Institut, Mannheim, 1972.

764

765   Kunz, A., Konopka, P., Müller, R., and Pan, L.L.: Dynamical tropopause based on

766   isentropic potential vorticity gradients, J. Geophys. Res., 116, D01110,

767   doi:10.1029/2010JD014343, 2011.

768

769   Lin, C.-J., Pongprueksa, P., Lindberg, S.E., Pehkonen, S.O., Byun, D., and Jang, C.:

770   Scientific uncertainties in atmospheric mercury models. I. Model science evaluation,

771   Atmos. Environ, 40, 2911-2928, 2006.

772

773   Lindberg, S., Bullock, R., Ebinghaus, R., Engstrom, D., Feng, X., Fitzgerald, W., Pirrone,

774   N., Prestbo, E., and Seigneur, C.: A synthesis of progress and uncertainties in attribution

775   the sources of mercury in deposition, Ambio, 36, 19-32, 2007.

776

777   Lyman, S.N., and Jaffe, D.A.: Formation and fate of oxidized mercury in the upper

778   troposphere and lower stratosphere, Nature Geosci., 5, 114-117, 2012.

779

780   Menzies, R.T., and Tratt, D.M.: Evidence of seasonally dependent stratosphere-

781   troposphere exchange and purging of lower stratospheric aerosol from a multiyear lidar

782   data set, J. Geophys. Res., 100, D2, 3139-3148, 1995.

783

784   Mergler, D., Anderson, H.A., Chan, L.H.M., Mahaffey, K.R., Murray, M., Sakamoto, M.,

785   and Stern, A.H.: Methyl mercury exposure and health effects in humans: A worldwide

786   concern, Ambio, 36, 3-11, 2007.

787

788   Murphy, D.M., Thomson, D.S., and Mahoney, M.J.: In situ measurements of organics,

789   meteoritic material, mercury, and other elements in aerosols at 5 to 19 kilometers,

790   Science, 282, 1664-1669, 1998.

791

792   Murphy, D.M., Hudson, P.K., Thomson, D.S., Sheridan, P.J., and Wilson, J.C.:

793   Observations of mercury-containing aerosols, Environ. Sci. Technol., 40, 3163-3167,

794   2006.

795

796   Nevison, C.D., Dlugokencky, E., Dutton, G., Elkins, J.W., Fraser, P., Hall, B., Krummel,

797   P.B., Langenfelds, R.L., O´Doherty, S., Prinn, R.G., Steele, L.P., and Weiss, R.F.:

798   Exploring causes of interannual variability in the seasonal cycles of tropospheric nitrous

799   oxide, Atmos. Chem. Phys., 11, 3713-3730, 2011.

800

801   Pirrone, N., Cinnirella, S., Feng, X., Finkelman, R.B., Friedli, H.R., Leaner, J., Mason,

802   R., Mukherjee, A.B., Stracher, G.B., Streets, D.G., and Telmer, K.: Global mercury

803   emissions to the atmosphere from anthropogenic and natural sources, Atmos. Chem.

804   Phys., 10, 5951-5964, 2010.

805

806   Radke, L.F., Friedli, H.R., and Heikes, B.G.: Atmospheric mercury over the NE Pacific

807   during spring 2002: Gradients, residence time, upper troposphere lower stratosphere loss,

808   and long-range transport, J. Geophys. Res., 112, D19305, doi:10.1029/2005JD005828,

809   2007.

810

811   Rasch, P.J., Tilmes, S., Turco, R.P., Robock, A., Oman, L., Chen, C.-C., Stenchikov,

812   G.L., and Garcia, R.R.: An overview of geoengineering of climate using stratospheric

813   sulphate aerosols, Phil. Trans. R. Soc. A, 366, 4007-4037, 2008.

814

815   Rutter, A.P., and Schauer, J.J.: The effect of temperature on the gas-particle partitioning

816   of reactive mercury in atmospheric aerosols, Atmos. Environ., 41, 8647-8657, 2007.

817

818   Scheele, M., Siegmund, P., and Van Velthoven, P.: Sensitivity of trajectories to data

819   resolution and its dependence on the starting point: In or outside a tropopause fold,

820   Meteorol. Appl., 3, 267-273, 1996.

821

822   Scheuhammer, A.M., Meyer, M.W., Sandheinrich, M.B., and Murray, M.W.: Effects of

823   environmental methylmercury on the health of wild bird, mammals, and fish, Ambio, 36,

824   12-18, 2007.

825

826   Selin, N.E., Jacob, D.J., Park, R.J., Yantosca, R.M., Strode, S., Jaeglé, L., and Jaffe, D.:

827   Chemical cycling and deposition of atmospheric mercury: Global constraints from

828   observations, J. Geophys. Res., 112, D02308, doi:10.1029/2006JD007450, 2007.

829

830   Slemr, F., Ebinghaus, R., Brenninkmeijer, C.A.M., Hermann, M., Kock, H.H.,

831   Martinsson, B.G., Schuck, T., Sprung, D., van Velthoven, P., Zahn, A., and Ziereis, H.:

832   Gaseous mercury distribution in the upper troposphere and lower stratosphere observed

833   onboard the CARIBIC passenger aircraft, Atmos. Chem. Phys., 9, 1957-1969, 2009.

834

835   Slemr, F., Weigelt, A., Ebinghaus, R., Brenninkmeijer, C., Baker, A., Schuck, T., Rauthe-

836   Schöch, A., Riede, H., Leedham, E., Hermann, M., van Velthoven, P., Oram, D.,

837   O´Sullivan, D., Dyroff, C., Zahn, A., and Ziereis, H.: Mercury plumes in the global upper

838   troposphere observed during flights with the CARIBIC observatory from May 2005 until

839   June 2013, Atmosphere 5, 342-369, 2014.

840

841   Slemr, F., Weigelt, A., Ebinghaus, R., Kock, H.H., Bödewadt, J., Brenninkmeijer,

842   C.A.M., Rauthe-Schöch, A., Weber, S., Hermann, M., Becker, J., Zahn, A., and

843   Martinsson, B.: Atmospheric mercury measurements onboard the CARIBIC passenger

844   aircraft, Atmos. Meas. Tech., 9, 2291-2302, 2016.

845

846   Sprung, D., and Zahn, A.: Acetone in the upper troposphere/lowermost stratosphere

847   measured by the CARIBIC passenger aircraft: Distribution, seasonal cycle, and

848   variability, J. Geophys. Res., 115, D16301, doi:10.1029/2009JD012099, 2010.

849

850   Swartzendruber, P.C., Jaffe, D.A., Prestbo, E.M., Weiss-Penzias, P., Selin, N.E., Park, R.,

851   Jacob, D.J., Strode, S., and Jaeglé, L.: Observations of reactive gaseous mercury in the

852   free troposphere at the Mount Bachelor Observatory, J. Geophys. Res., 111, D24301,

853   doi:10.1029/2006JD007415, 2006.

854

855   Swartzendruber, P.C., Chand, D., Jaffe, D.A., Smith, J., Reidmiller, D., Gratz, L., Keeler,

856   J., Strode, S., Jaeglé, L., and Talbot, R.: Vertical distribution of mercury, CO, ozone, and

857   aerosol scattering coefficient in the Pacific Northwest during the spring 2006 INTEX-B

858   campaign, J. Geophys. Res., 113, D10305, doi:10.1029/2007JD009579, 2008.

859

860   Swartzendruber, P.C., Jaffe, D.A., and Finley, B.: Improved fluorescence peak

861   integration in the Tekran 2537 for applications with sub-optimal sample loadings, Atmos.

862   Environ., 43, 3648-3651, 2009.

863

864   Talbot, R., Mao, H., Scheuer, E., Dibb, J., and Avery, M.: Total depletion of Hg^0 in the

865   upper troposphere – lower stratosphere, Geophys. Res. Lett., 34, L23804,

866   doi:10.1029/2007GL031366, 2007a.

867

868   Talbot, R., Mao, H., Scheuer, E., Dibb, J., Avery, M., Browell, E., Sachse, G., Vay, S.,

869   Blake, D., Huey, G., and Fuelberg, H.: Factors influencing the large-scale distribution of

870   Hg^o in the Mexico City area and over the North Pacific, Atmos. Chem. Phys. Discuss., 7,

871   15533-15563, 2007b.

872

873   Travnikov, O., Angot, H., Artaxo, P., Bencardino, M., Bieser, J., D´Amore, F., Dastoor,

874   A., De Simone, F., Carmen Diéguez, M., Dommergue, A., Ebinghaus, R., Feng, X.B.,

875   Gencarelli, C.N., Hedgecock, I.M., Magand, O., Martin, L., Matthias, V., Mashyanov, N.,

876   Pirrone, N., Ramachandran, R., Read, K.A., Ryjkov, A., Selin, N.E., Sena, F., Song, S.,

877   Sprovieri, F., Wip, D., Wängberg, I., and Yang, X.: Multi-model study of mercury

878   dispersion in the atmosphere: atmospheric processes and model evaluation, Atmos.

879   Chem. Phys., 17, 5271-5295, 2017.

880

881   Volk, C.M., Elkins, J.W., Fahey, D.W., Dutton, G.S., Gilligan, J.M., Loewenstein, M.,

882   Podolske, J.R., Chan, K.R., and Gunson, M.R.: Evaluation of source gas lifetimes from

883   stratospheric observations, J. Geophys. Res. 102, D21, 25543-25564, 1997.

884

885   Weigelt, A., Ebinghaus, R., Pirrone, N., Bieser, J., Bödewadt, J., Esposito, G., Slemr, F.,

886   van Velthoven, P.F.J., Zahn, A., and Ziereis, H.: Tropospheric mercury vertical profiles

887   between 500 and 10000 m in central Europe, Atmos. Chem. Phys., 16, 4135-4146, 2016a.

888

889   Weigelt, A., Slemr, F., Ebinghaus, R., Pirrone, N., Bieser, J., Bödewadt, J., Esposito, G.,

890   and van Velthoven, P.F.J.: Mercury emissions of a coal-fired power plant in Germany,

891   Atmos. Chem. Phys., 16, 13653-13668, 2016b.

892

893   Wilson, J.C., Lee, S.-H., Reeves, J.M., Brock, C.A., Jonsson, H.H., Lafleur, B.G.,

894   Loewenstein, M., Podolske, J., Atlas, E., Boehring, K., Toon, G., Fahey, D., Bui, T.P.,

895   Diskin, G., and Moore, F.: Steady-state aerosol distributions in the extra-tropical, lower

896   stratosphere and the processes that maintain them, Atmos. Chem. Phys., 8, 6617-6626,

897   2008.

898

Figures

Figure 1: Tracks of the CARIBIC flights made beetween April 2014 and February 2016 (CARIBIC flights #468-536). Mercury data for these flights were obtained by post-flight processing of the Tekran raw signal (Slemr et al., 2016).
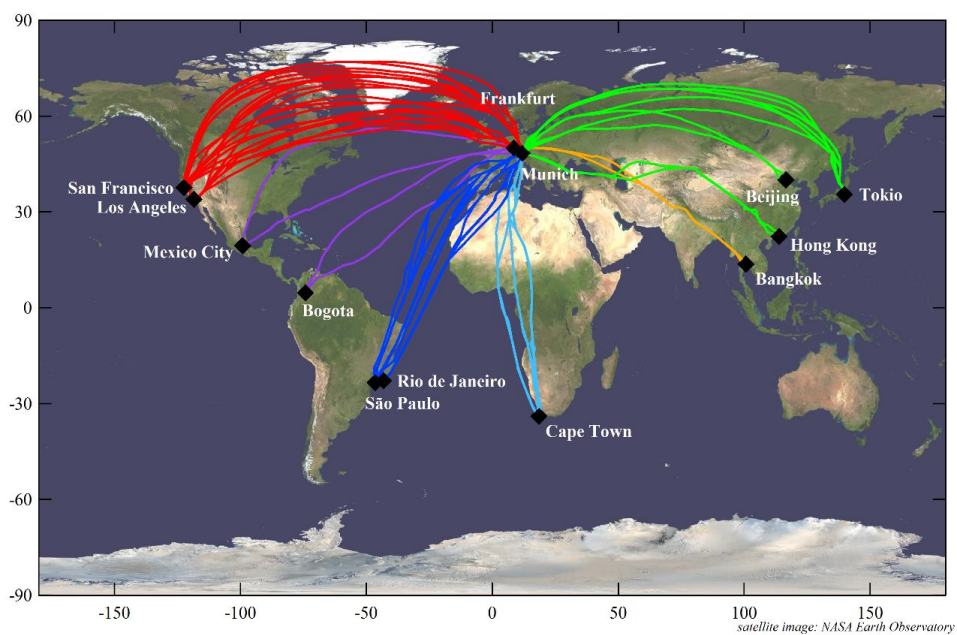
908 Figure 2: Latitudinal distributions of tropospheric (PV ≤ 1.5 PVU) TM, CO, CH$_4$, and
909 acetonitrile (AN) during the flights from Bogota and São Paulo/Rio de Janeiro to Munich
910 in summer (only July and August, JA), autumn (September, October, and November,
911 SON) and winter (December, January, and February, DJF). The points represent averages
912 and the vertical bars their standard error. No acetonitrile data were available south of
913 20°S.
914
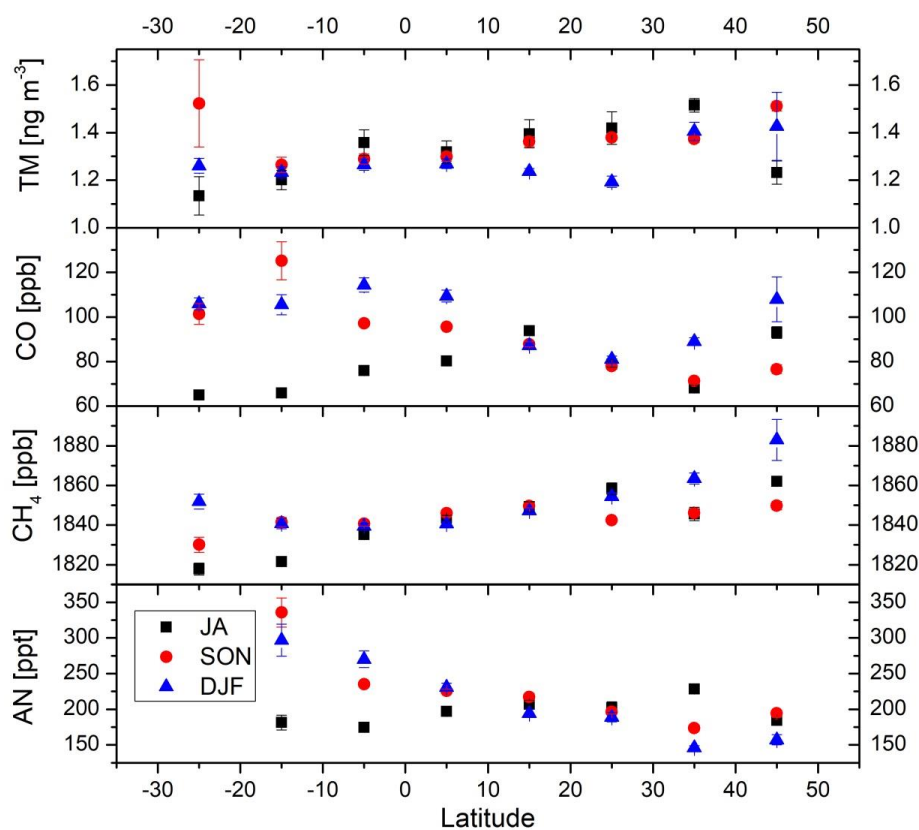
915
916
917

918   Figure 3: Latitudinal distributions of tropospheric TM, CO, CH$_4$, and acetonitrile (AN) in
919   winter (December, January, and February, DJF) during the flights from Cape Town and
920   São Paulo to Munich. The points represent averages and the vertical bars their standard
921   error. No acetonitrile data are available south of 30°S and 20°S for flights to Cape Town
922   and São Paulo, respectively.
923
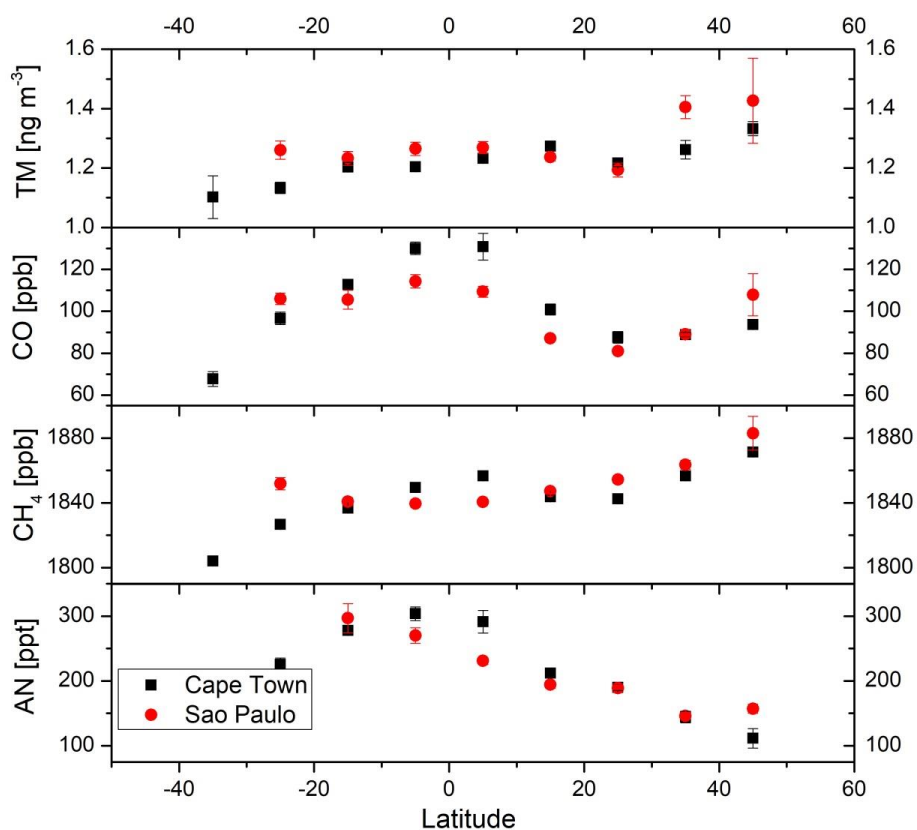
924
925

926   Figure 4: Seasonal variation of mean TM concentrations (a), CO (b), CH$_4$ (c) and O$_3$ (d)
927   mixing ratios in distance relative to the thermal tropopause derived from ozone soundings
928   according to Sprung and Zahn (2010). All TM data north of 20°N obtained between April
929   2014 and February 2016 were considered for this plot (2288 individual data points).
930
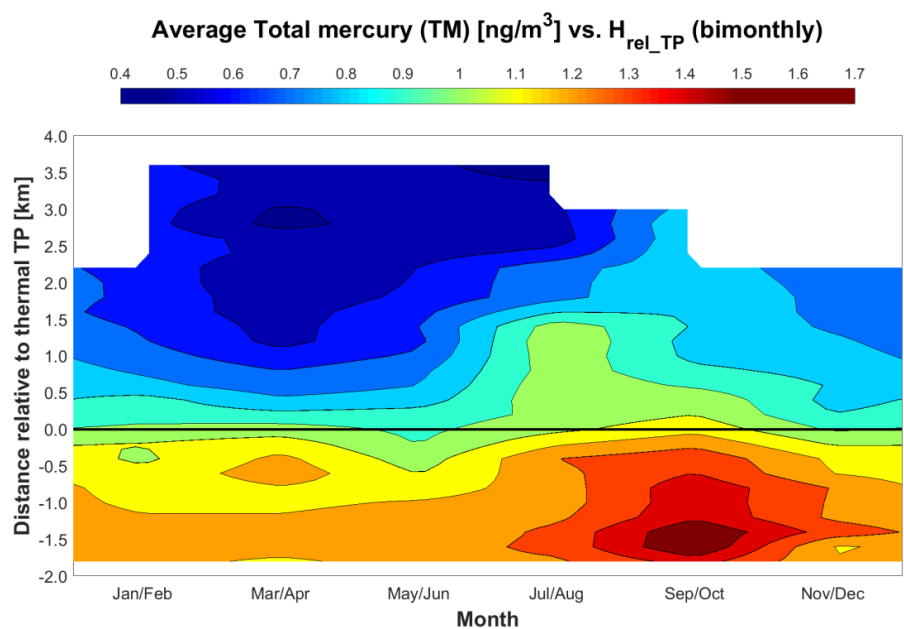
931
932
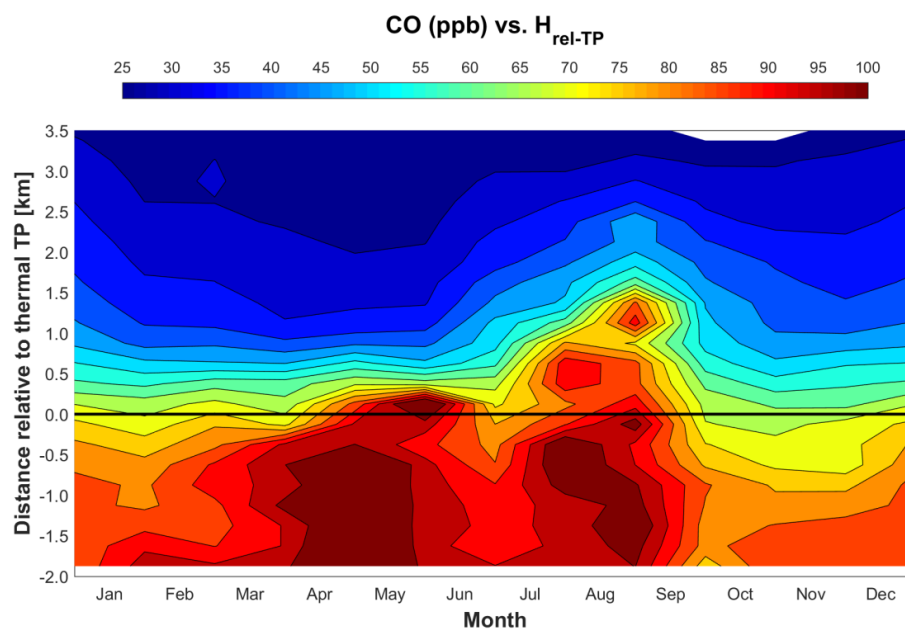
933
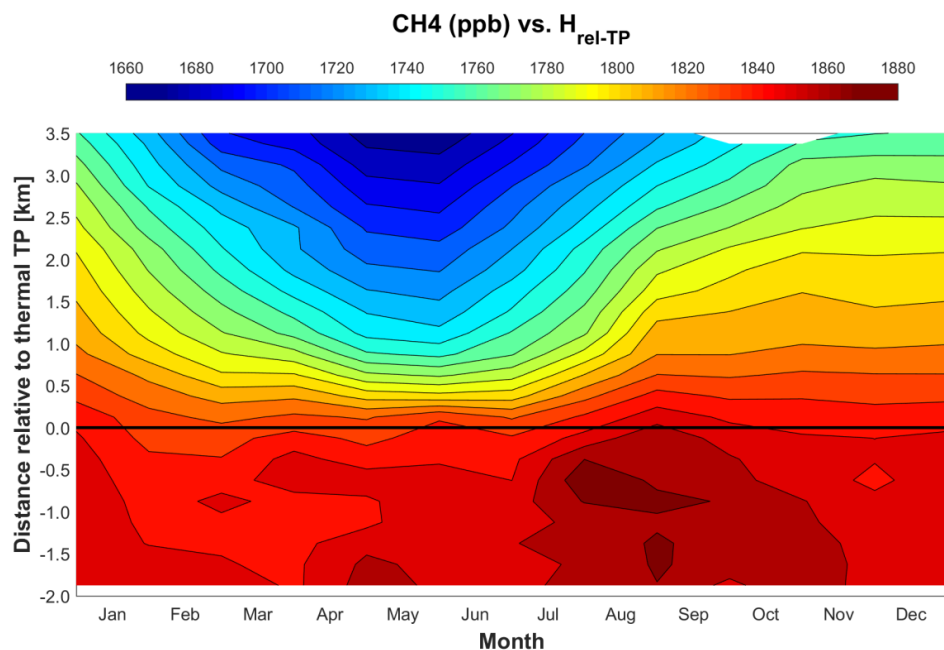
934
935
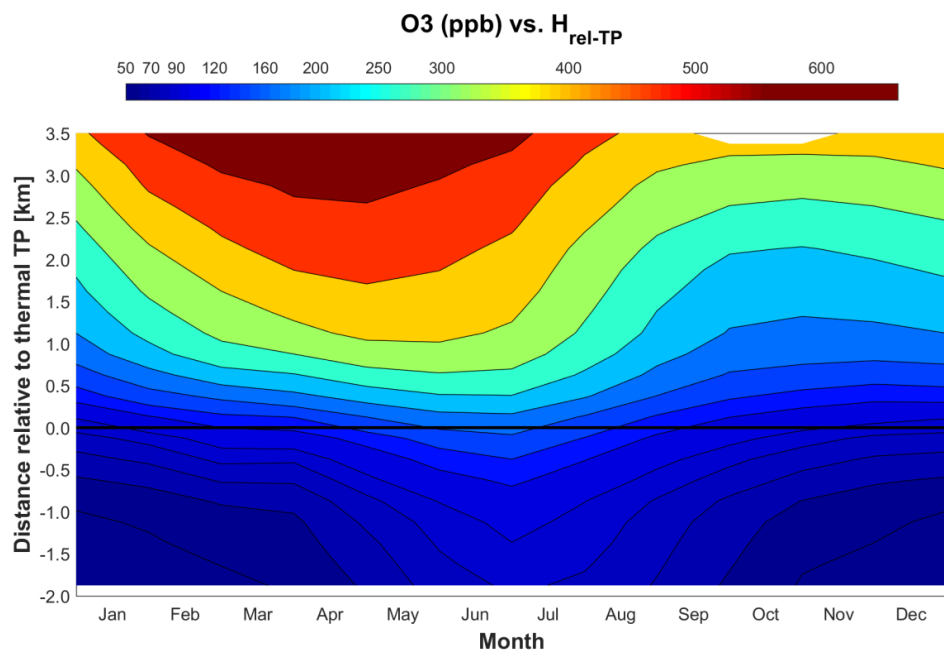
936

937   Figure 5: Vertical TM and GEM distribution relative to the thermal tropopause in a)
938   winter (December – May, upper panel) and b) in summer (June – November, lower
939   panel). The data points represent averages and their standard errors, extreme values were
940   eliminated using the Nalimov outlier test (Kaiser and Gottschalk, 1972).
941
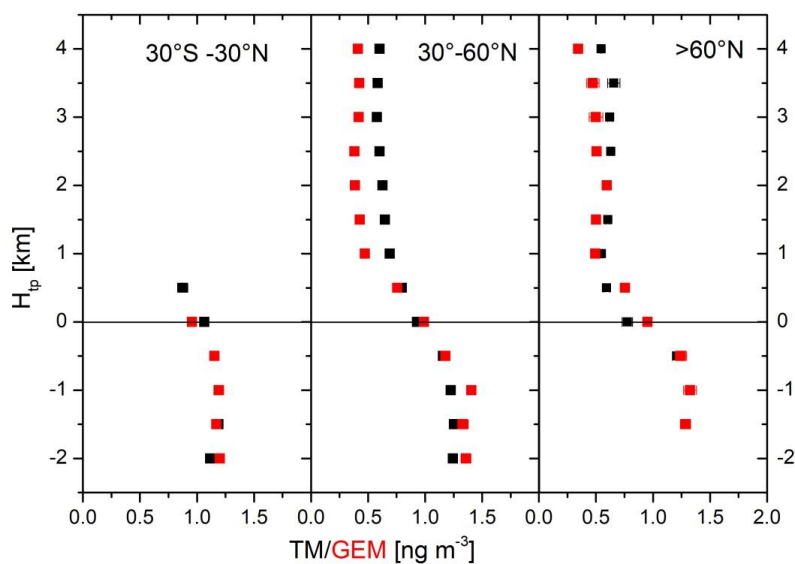
942
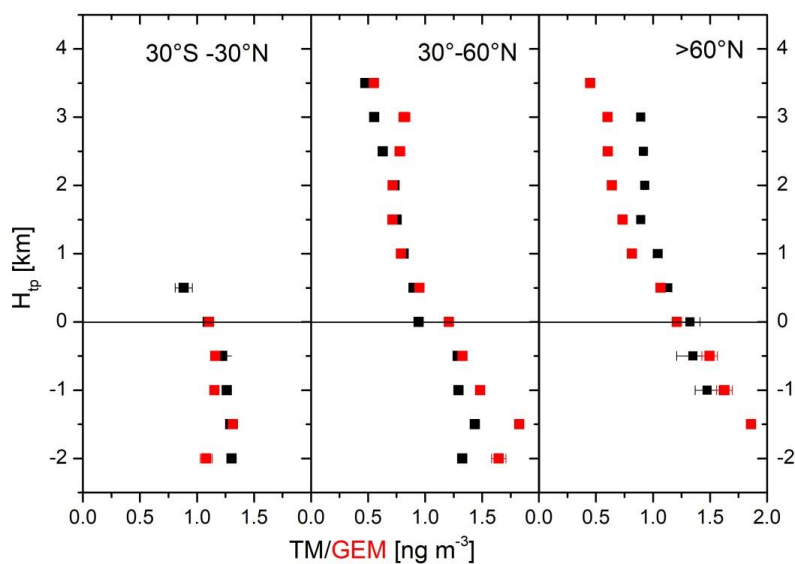
943
944

945
946   Figure 6: Stratospheric average TM and GEM concentrations in boreal winter (November
947   – April) are binned according to the N_2O mixing ratio. N_2O mixing ratios were detrended
948   using 2015 as a reference year and the N_2O growth rate of 0.844 ppb yr^{-1} (Assonov et al.,
949   2013). Vertical and horizontal bars represent the standard errors of the averages.
950

951